

GA-A27923

ACHIEVING STEADY-STATE CONDITIONS IN HIGH-BETA HYBRID SCENARIO IN DIII-D

by

C.C. PETTY, F. TURCO, M.A. VAN ZEELAND, C.T. HOLCOMB, J.E. KINSEY,
T.C. LUCE, J.R. FERRON, E.J. DOYLE, A.M. GAROFALO, A.W. HYATT,
G.L. JACKSON, W.M. SOLOMON, AND Y. ZHU

SEPTEMBER 2014



DISCLAIMER

This report was prepared as an account of work sponsored by an agency of the United States Government. Neither the United States Government nor any agency thereof, nor any of their employees, makes any warranty, express or implied, or assumes any legal liability or responsibility for the accuracy, completeness, or usefulness of any information, apparatus, product, or process disclosed, or represents that its use would not infringe privately owned rights. Reference herein to any specific commercial product, process, or service by trade name, trademark, manufacturer, or otherwise, does not necessarily constitute or imply its endorsement, recommendation, or favoring by the United States Government or any agency thereof. The views and opinions of authors expressed herein do not necessarily state or reflect those of the United States Government or any agency thereof.

ACHIEVING STEADY-STATE CONDITIONS IN HIGH-BETA HYBRID SCENARIO IN DIII-D

by

C.C. PETTY¹, F. TURCO², M.A. VAN ZEELAND¹, C.T. HOLCOMB³, J.E. KINSEY⁴,
T.C. LUCE¹, J.R. FERRON¹, E.J. DOYLE⁵, A.M. GAROFALO¹, A.W. HYATT¹,
G.L. JACKSON¹, W.M. SOLOMON⁶, AND Y. ZHU⁷

This is a preprint of the synopsis for a paper to be presented at
the Twenty-Fifth IAEA Fusion Energy Conf., October 13-18, 2014
in Saint Petersburg, Russia.

¹General Atomics, P.O. Box 85608, San Diego, California, USA

²Columbia University, New York, New York, USA

³Lawrence Livermore National Laboratory, Livermore, California, USA

⁴CompX, Del Mar, California, USA

⁵University of California, Los Angeles, Los Angeles, California, USA

⁶Princeton Plasma Physics Laboratory, Princeton, New Jersey, USA

⁷University of California, Irvine, Irvine, California, USA

Work supported by
the U.S. Department of Energy under DE-FC02-04ER54698,
DE-FG02-04ER54761, DE-AC52-07NA27344, DE-FG03-99ER54541,
DE-FG02-08ER54984, DE-AC01-09CH11466, and DE-FG03-94ER54271

GENERAL ATOMICS PROJECT 30200
SEPTEMBER 2014

Achieving Steady-State Conditions in High-Beta Hybrid Scenario in DIII-D

PPC/P2-36

C.C. Petty 1), F. Turco 2), M.A. Van Zeeland 1), C.T. Holcomb 3), J.E. Kinsey 4),
T.C. Luce 1), J.R. Ferron 1), E.J. Doyle 5), A.M. Garofalo 1), A.W. Hyatt 1),
G.L. Jackson 1), W.M. Solomon 6) and Y. Zhu 7)

email: petty@fusion.gat.com

- 1) General Atomics, PO Box 85608, San Diego, CA 92186-5608, USA
- 2) Columbia University, 2960 Broadway, New York, NY 10027-6900, USA
- 3) Lawrence Livermore National Laboratory, 7000 East Ave, Livermore, CA 94550, USA
- 4) CompX, PO Box 2672, Del Mar, CA 92014, USA
- 5) University of California Los Angeles, PO Box 957099, Los Angeles, CA 90095-7099, USA
- 6) Princeton Plasma Physics Laboratory, PO Box 451, Princeton, NJ 08543-0451, USA
- 7) University of California at Irvine, Irvine, CA 92697-4575, USA

Abstract. The natural attributes of the hybrid scenario, especially the anomalously broad current profile that suppresses sawteeth by maintaining the safety factor minimum (q_{\min}) above unity, allows steady-state conditions with zero surface loop voltage to be achieved in 1.0 MA discharges in DIII-D with efficient central current drive and simultaneous high beta and high confinement. Approximately half of the plasma current is driven non-inductively near the plasma center by electron cyclotron waves and neutral beam injection, with the rest generated by the bootstrap current. The best steady-state discharges sustain normalized beta of 3.64, poloidal beta of 2.23, and H_{98y2} confinement factor of 1.56. A zero-dimensional physics model shows that steady-state hybrid operation with fusion gain $Q_{\text{fus}} \sim 4$ is feasible in FNSF and ITER.

1. Introduction to Steady-State Hybrid Regime

Experiments in DIII-D are demonstrating that the “hybrid” scenario is a viable steady-state advanced tokamak (AT) regime with central current drive and q_{\min} slightly above 1. This differs from the usual AT approach that leverages off-axis current drive to maintain $q_{\min} > 2$ for high bootstrap current fraction [1]. First developed as an inductively driven scenario, the hybrid regime is a long duration, high performance H-mode scenario that has higher confinement ($H_{98y2} = 1.6$) and greater stability ($\beta_N > 3$) to the $m/n=2/1$ tearing mode than the conventional H-mode regime. Several realizations of the hybrid scenario have been reported from the ASDEX-Upgrade [2], JET [3] and JT-60U [4] tokamaks, as well as from the DIII-D tokamak [5]. In DIII-D, the favorable properties of hybrids are largely attributed to the presence of a $m/n=3/2$ tearing mode that stabilizes the sawtooth and fishbone instabilities by raising q_{\min} slightly above 1 with low central magnetic shear [6].

In DIII-D, experiments show that the beneficial characteristics of hybrids are maintained when strong central current drive from electron cyclotron (EC) waves and neutral beam injection (NBI) is applied to increase the non-inductive fraction to $\approx 100\%$. The advantages of the hybrid regime over the $q_{\min} > 2$ AT regime are (1) good alignment between the current drive and plasma current profiles is not necessary as poloidal magnetic flux pumping self-organizes the current density profile in hybrids with an $m/n=3/2$ tearing mode [7], and (2) the current drive in hybrids can be located near the plasma center where the current drive efficiency is highest. The high current drive efficiency can fully compensate for the lower bootstrap current fraction in the $q_{\min} \approx 1$ hybrid regime compared to the $q_{\min} > 2$ AT regime.

The hybrid plasmas discussed in this paper use a combination of on-axis and off-axis NBI to broaden the fast ion pressure profile. Stability studies have shown that the ideal with-wall $n=1$ limit increases with a broader pressure profile for plasmas with $q_{\min}=1$ [8,9], so off-axis NBI may be advantageous for increasing β_N in the hybrid scenario. In addition, a broadened fast ion pressure profile should have increased stability to Alfvén eigenmodes (AEs) [10].

2. Steady-State Hybrid Plasmas in DIII-D

The potential of the hybrid scenario as a robust regime for high-beta, steady-state plasmas is seen in Fig. 1, where three consecutive discharges achieve essentially zero surface loop voltage, normalized beta up to $\beta_N=3.64$ and toroidal beta up to $\beta_T=3.1\%$ for the full duration of the NBI pulse without exciting the deleterious $m/n=2/1$ tearing mode. The current relaxation time [11] is calculated to be $\tau_R=1.75$ s at the maximum heating power. Using the 6 available gyrotrons, 3.1 MW of co-current drive power is absorbed at the second harmonic resonance near the plasma center. All six of the co-neutral beam sources are utilized with a peak injected power of 11.0 MW; two of the beams are vertically tilted for off-axis deposition. The plasma shape is a double-null-divertor (DND) vertically biased away from the ∇B -drift direction; this direction of vertical shift yields a 15% higher value of H_{98y2} compared to cases with the opposite vertical shift.

Table 1. Hybrid parameters for two point scan in magnetic field and plasma current with $P_{NBI} = 10.6$ MW and $P_{EC} = 2.3$ MW.

		B_T (T)	
		1.7	1.9
I_p (MA)	1.0	$\beta_N = 3.40$ $\beta\tau = 0.27\%s$ $H_{98y2} = 1.23$ $V_{surf} = 8$ mV	$\beta_N = 3.17$ $\beta\tau = 0.25\%s$ $H_{98y2} = 1.30$ $V_{surf} = 4$ mV
	1.1	$\beta_N = 3.15$ $\beta\tau = 0.28\%s$ $H_{98y2} = 1.18$ $V_{surf} = 34$ mV	$\beta_N = 3.23$ $\beta\tau = 0.30\%s$ $H_{98y2} = 1.40$ $V_{surf} = 19$ mV

There is no evidence that a stability limit is reached in these steady-state hybrid plasmas, including no evidence for any confinement factor degradation at high beta. As seen in Fig. 2(a), normalized beta increases steadily with increasing heating power. A small two-point scan in B_T and I_p , shown in Table 1, has been done to optimize plasma performance and non-inductive current fraction in plasmas that are vertically biased towards the ∇B -drift direction. Examining the discharges with the same q_{95} value, i.e., $\{B_T=1.7$ T, $I_p=1.0$ MA $\}$ and $\{B_T=1.9$ T, $I_p=1.1$ MA $\}$, the confinement factor and fusion gain ($\beta\tau$) are seen to be slightly larger at higher field, but slightly larger β_N is achieved at lower field. The biggest difference between the discharges in Table 1 is the surface loop voltage (V_{surf}), which is a critical quantity for steady-state operation with the $\{B_T=1.9$ T, $I_p=1.0$ MA $\}$ case coming closest to being fully non-inductive.

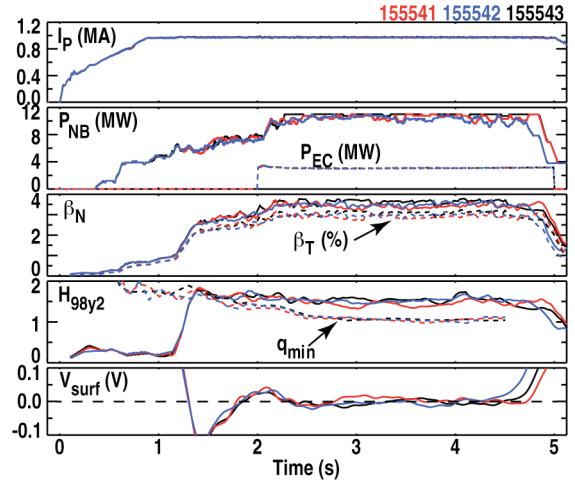


Fig. 1. Time history of three consecutive steady-state hybrid discharges.

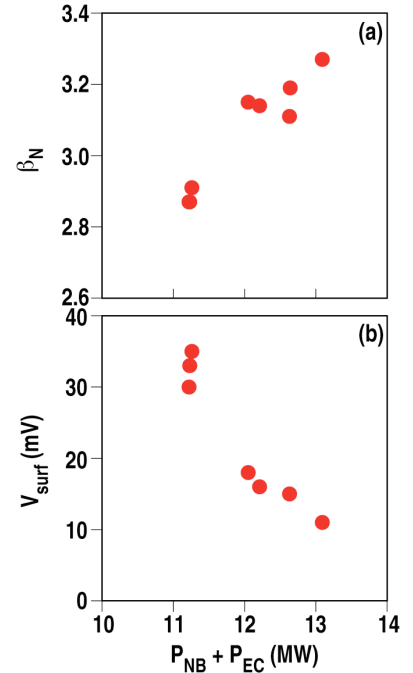


Fig. 2. (a) Normalized beta and (b) surface loop voltage vs. total heating power.

2.1. Non-inductive current analysis

A good indicator of 100% non-inductive current is zero surface loop voltage for longer than a current relaxation time. As seen in Fig. 2(b), the measured V_{surf} decreases with increasing heating power in hybrids, which is expected owing to the larger external current drive and larger bootstrap current. Figure 3 shows that, for a fixed co-NBI power of 11.0 MW, V_{surf} is driven down to zero for up to $2\tau_R$ when the poloidal beta is increased above 1.9 by raising the EC power to 3.1 MW and reducing I_p from 1.1 MA to 1.0 MA.

Zero surface loop voltage is consistent with the calculated non-inductive current, but the reconstructed current profile does not agree with the simple sum of the calculated current drive profiles. As seen in Table 2 for a discharge with $\beta_N=3.64$ and $V_{\text{surf}}=-0.003$ V, hybrids can have close to 50% bootstrap current fraction despite $q_{\text{min}}\approx 1$; the other half of the plasma current is driven efficiently using central EC and NBI current drive. Electron cyclotron waves are calculated to be 2.5 times more effective at central current drive than NBI. The high on-axis current drive efficiency compensates for the moderate bootstrap current fraction. The hybrid current profile remains broad despite the strong central current drive. Figure 4(a) shows that the sum of the non-inductive current profiles (EC, NBI and bootstrap current) is more peaked than the total current profile determined from an equilibrium reconstruction constrained by MSE polarimetry. The current profile anomaly is displayed in Fig. 4(b), where the calculated non-inductive current density is subtracted from the total current density determined by a well-constrained EFIT equilibrium reconstruction. The current profile is strongly overdriven between $\rho=0.05$ and $\rho=0.2$ and the current relaxation time is sufficiently short that q_{min} should drop below 1 by the end of the discharge. The fact that q_{min} remains above unity and sawteeth are suppressed shows that the hybrid scenario maintains an anomalously broad current profile even in the presence of strong central current drive. The anomalous redistribution of current may also be responsible for filling in the “current hole” inside $\rho=0.05$.

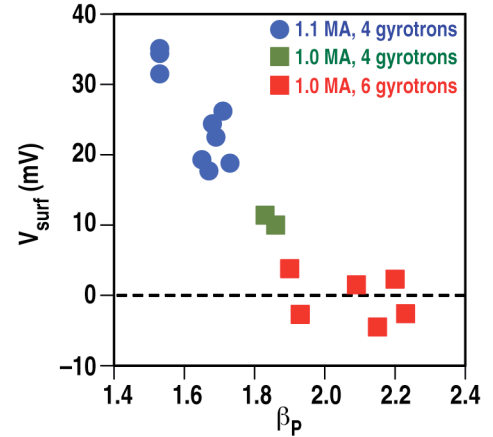


Fig. 3. Measured surface loop voltage as a function of β poloidal in hybrids with central current drive.

Table 2. Calculated non-inductive currents for hybrid plasma with $P_{\text{NBI}}=11.0$ MW and $P_{\text{EC}}=3.1$ MW.

I_{EC}	0.21 MA
I_{NBI}	0.30 MA
I_{BS}	0.46 MA
I_{NI}	0.97 ± 0.05 MA
I_p	0.97 MA

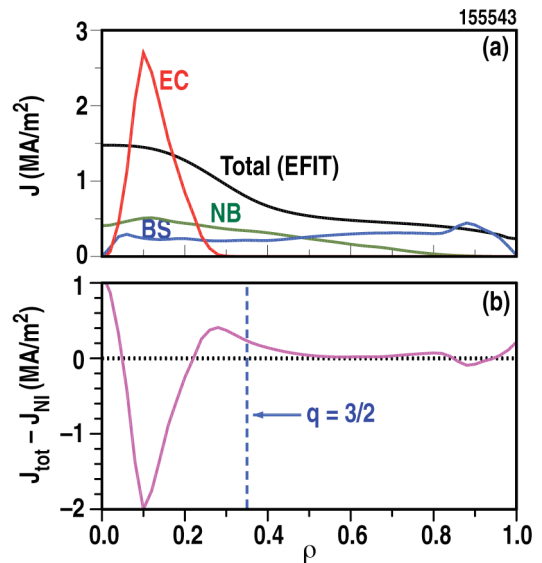


Fig. 4. (a) Total current density from EFIT, and modeled current density from EC, NBI and bootstrap. (b) Difference between total current density from EFIT and modeled non-inductive current densities.

2.2. Stability analysis

The beta value obtained at the maximum current drive power available for these experiments is close to the calculated ideal with-wall $n=1$ limit. The theoretical stability limits are calculated by the DCON code [12] using EFIT reconstructions constrained by the experimental pressure profile, MSE polarimetry and a neoclassical calculation of the pedestal bootstrap current density. To allow DCON to determine the $n=1$ limit, the EFIT reconstruction is adjusted to keep $q_{\min} > 1.03$. Figure 5 shows that in steady-state hybrids a high value of $\beta_N/I_i = 4.9$ is reached and maintained for the duration of high power NBI. This value exceeds the no-wall $n=1$ stability limit (average DCON value $\beta_N/I_i = 4.0$) and is close to the ideal with-wall $n=1$ limit. There is considerable scatter in the ideal with-wall $n=1$ limit displayed in Fig. 5 which makes a detailed comparison difficult, but the average value for all time slices is $\beta_N/I_i = 5.3$. Future experiments will try to achieve $\beta_N/I_i \geq 5.5$ for long pulses to test this predicted limit.

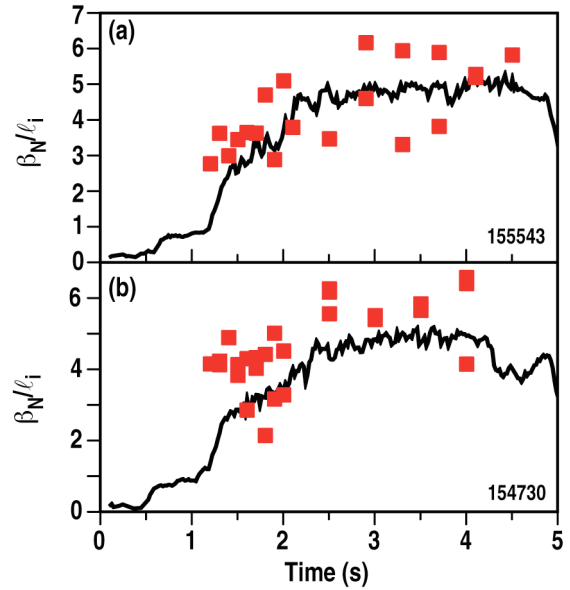


Fig. 5. Measured β_N/I_i in steady-state hybrids (solid line) compared to DCON calculations of the ideal with-wall $n=1$ limits (red squares) for (a) $I_p = 1.0$ MA, $n_{19} = 4.1$ and (b) $I_p = 1.1$ MA, $n_{19} = 4.8$.

Most of the steady-state hybrid plasmas have some level of discernible coherent mode activity in the Alfvén eigenmode frequency range during the high beta phase. Mode activity is investigated using the crosspower of vertical and radial CO_2 interferometer chords, electron cyclotron emission (for 1.9 T discharges), and magnetic probes. Interferometer spectrograms are shown in Fig. 6 for a two-point scan in B_T and I_p . For reference, the approximate toroidal Alfvén eigenmode (TAE) frequency at q_{\min} is plotted in each panel. The discharge shown in Fig.

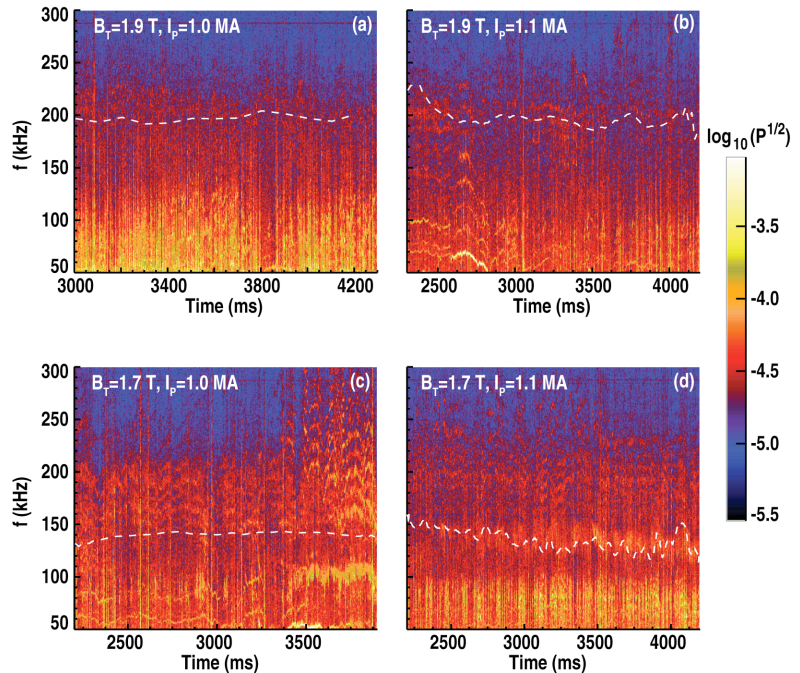


Fig. 6. Spectrograms from CO_2 interferometers for two-point scan of B_T and I_p in steady-state hybrids. Dash lines indicate approximate TAE frequency at q_{\min} .

6(a) has the least amount of AE activity, and interestingly is the highest performance case from these experiments ($\beta_N = 3.64$, $H_{98y2} = 1.56$ and $V_{\text{surf}} = -0.003$ V). Additionally, a comparison of the neutron scintillator detectors with a zero-dimensional neutron prediction shows good agreement (within 6%), suggesting there is minimal anomalous transport of beam ions for this case. The remaining discharges in Fig. 6 all show clear evidence of TAE modes, with the

$B_T=1.7$ T cases showing more AE activity than the $B_T=1.9$ T cases. The neutron emission is anti-correlated with AE activity, with the neutron scintillator detectors measuring 26% below the zero-dimensional neutron prediction for Fig. 6(d), while for Fig. 6(b) the discrepancy is only 19%. Figure 6(c) has the largest mode amplitude and a significantly different spectrum of modes. This difference is most obvious after 3.4 s where a spectrum of TAEs up to 300 kHz appear, as well as a lower frequency rapidly chirping mode near ~ 100 kHz. While Fig. 6(c) has the largest neutron degradation at 34%, the new modes after 3.4 s cause no additional reduction in neutron emission relative to earlier portions of the discharge.

While the $m/n=3/2$ tearing mode activity in steady-state hybrids is ubiquitous (and beneficial, given its role in anomalously broadening the current profile [6,7]), the $n=1$ tearing mode behavior changes as β_N increases. As shown in Fig. 7(a), a $m/n=1/1$ mode appears in hybrid plasmas with $\beta_N=3.2$ when q_{\min} approaches 1, but no sawteeth are observed. Increasing β_N to 3.4 results in $m/n=1/1$ mode activity at higher frequency, as seen in Fig. 7(b). The change in mode frequency is attributed to a change in the safety factor profile, as seen in Fig. 7(c) using equilibrium reconstructions constrained by motional Stark effect (MSE) data. For the $\beta_N=3.2$ case the q profile is slightly reversed, with the measured toroidal rotation frequency of carbon ions from charge exchange recombination (CER) spectroscopy at the q_{\min} location ($\rho=0.21$) being in good agreement with the $m/n=1/1$ mode frequency (13 kHz). For the $\beta_N=3.4$ case the q profile becomes more monotonic, and the higher $m/n=1/1$ mode frequency (22 kHz) is in agreement with the higher toroidal rotation frequency of carbon ions at the new q_{\min} location ($\rho=0.02$). Finally, a $m/n=3/1$ mode occasionally appears in hybrids with $\beta_N \geq 3.4$, as seen in Fig. 7(b). The effect of this mode on the plasma parameters varies from having no detectable effect to a 10% reduction in beta, depending upon the mode size.

2.3. Transport analysis

The thermal energy confinement time in these steady-state hybrids is excellent. Even with electron heating from EC, confinement factors of up to $H_{98y2}=1.6$ are achieved. The highest confinement factors are obtained when the DND shape is biased downward, away from the ∇B -drift direction. Figure 8 compares two steady-state hybrid discharges (both with $V_{\text{surf}} < 0$) that have the same heating and current drive power but are vertically biased in opposite directions. It is seen that H_{98y2} and β_N are markedly higher for the downward shifted case. A power balance transport analysis of these two discharges during the high β_N phase is shown in Fig. 9. Outside $\rho=0.3$ there is a large reduction in the ion thermal diffusivity (χ_i), and a small reduction in the electron thermal diffusivity (χ_e), for the downward shifted case. The improved transport is likely due to a combination of higher $E \times B$ shear and higher density.

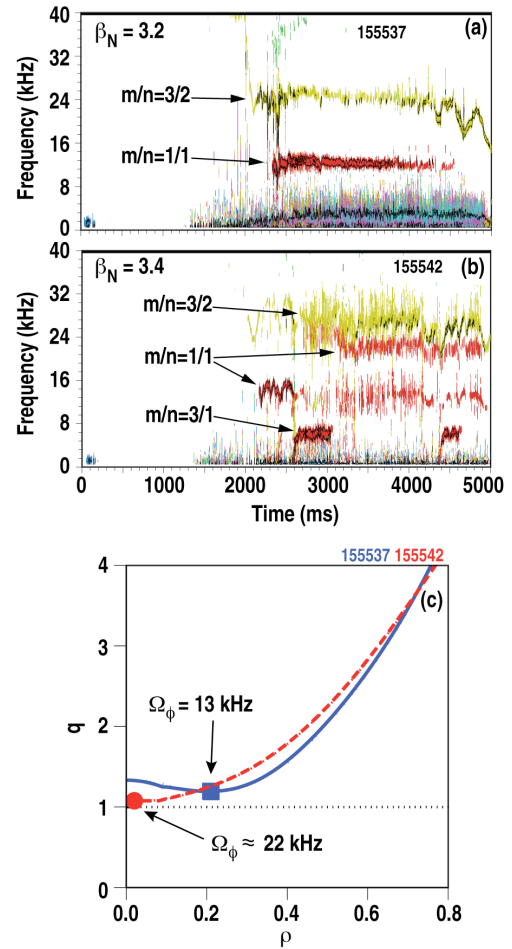


Fig. 7. Spectrograms from magnetic probes in steady-state hybrids with (a) $\beta_N=3.2$ and (b) $\beta_N=3.4$. The safety factor profiles from MSE-constrained EFIT reconstruction for these two discharges are shown in (c).

The increase in toroidal rotation rate when the DND shape is vertically shifted opposite to the ∇B -drift direction has been seen before in hybrid plasmas, which yields higher $E \times B$ shear that helps to suppress long wavelength turbulence. The density increases for plasmas biased away from the ∇B -drift direction because the divertor cryopumping is less effective. In these steady-state hybrid experiments there is a correlation between higher density and higher H_{98y2} factor that needs to be further investigated to determine the mechanism.

It should also be noted in Fig. 9 that χ_e is larger than χ_i for the downward shifted case. Since the ion and electron heat fluxes are nearly equal, this difference between the ion and electron thermal transport results in the ion temperature (T_i) being $\sim 50\%$ higher than the electron temperature (T_e). To make up this difference, i.e., to achieve $T_e = T_i$, the EC power either needs to be substantially increased or a steady-state hybrid regime needs to be developed with $\chi_e \approx \chi_i$. Previous steady-state hybrid discharges in the ITER similar shape (ISS) exhibit more equal electron and ion thermal transport than the DND shape used in these experiments. Simulations of the electron density and temperature profiles using the TGLF transport model predict that the peaked density profile for the ISS case is stabilizing for the electron temperature gradient (ETG) mode and should result in lower electron thermal transport. Future experiments in DIII-D will test in more detail the dependence of χ_e and χ_i on plasma shape in the steady-state hybrid regime. It should be noted that including finite beta effects in the TGLF modeling has a mild stabilizing effect, while the temperature profiles (at fixed density) are predicted to decrease by 12% on average if the $E \times B$ shear effect is turned off in TGLF.

3. Extrapolation to Burning Plasma Devices

The high- β hybrid extrapolates favorably to steady-state scenarios in FNSF and ITER, as demonstrated in this section using a zero-dimensional physics model [13]. Since the bootstrap current fraction is limited to $f_{BS} \leq 0.6$ in these $q_{min} \approx 1$ plasmas, the current drive efficiency is a critical model parameter. Here we use the central EC current drive efficiency specified in the ITER Physics Basis [14], $\gamma_{CD} = I_{CD} n_{19} R / P_{CD} = 2.5 \times 10^{19}$ A/m²W at $T_e = 20$ keV, to examine the feasibility of steady-state hybrids in burning plasma devices. The model input geometry, B_T , I_p and β_N are chosen to match the desired steady-state scenario in either FNSF or ITER. The H_{98y2} factor and plasma profile shapes are taken Ref. [13] (which agree well with the obtained values in DIII-D), as is the high Z impurity factor. The zero-dimensional physics model self-consistently determines the remaining parameters, i.e., T , f_{BS} , He ash, P_{fus} , P_{CD} , which is

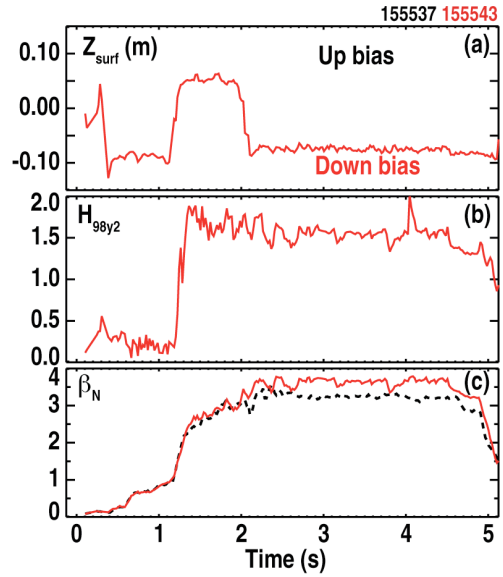


Fig. 8. Comparison of two hybrids ($P_{NBI}=11.0$ MW, $P_{EC}=3.1$ MW) that are vertically biased in different directions: (a) average height of plasma surface, (b) H_{98y2} confinement factor, and (c) normalized beta.

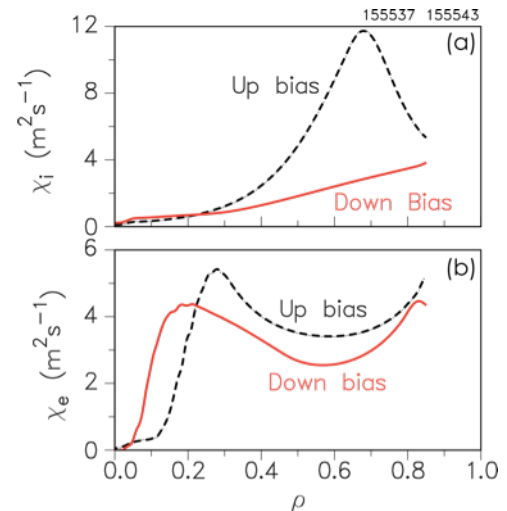


Fig. 9. Power balance transport analysis for the discharges shown in Fig. 8: (a) ion thermal diffusivity, and (b) electron thermal diffusivity.

enough to determine feasibility. To determine an attractive operating point, n_e is scanned at fixed β in the zero-dimensional physics model until the required auxiliary heating power equals the 100% non-inductive current drive power. Operating at this maximum permissible density value yields the highest fusion energy gain (Q_{fus}).

The operating parameters for steady-state hybrids in D-T plasmas on FNSF and ITER are shown in Table 3; the parameters for a steady-state hybrid (deuterium) plasma in DIII-D are also given for comparison. The FNSF mission is to develop fusion blankets and test materials with high neutron fluence and 30% availability in a modest-sized device with 100 to 250 MW fusion power and modest energy gain ($Q_{\text{fus}} < 5$) [13]. Currently the FNSF proposal calls for current drive at the plasma's half radius to create a q profile with weak negative magnetic shear; however, Table 3 shows that attractive operating parameters also exist for FNSF in the hybrid scenario that have the required neutron wall loading and $Q_{\text{fus}} = 3.5$. It is noteworthy that fully non-inductive hybrids in DIII-D have essentially achieved the needed FNSF values of β_N , H_{98y2} and density normalized to the Greenwald limit (n_e/n_{GW}).

Table 3. Steady-state hybrid parameters from a zero-dimensional physics model for FNSF and ITER. Achieved parameters in DIII-D are shown for comparison.

	DIII-D	FNSF	ITER
R (m)	1.68	2.49	6.2
R/a	2.9	3.5	3.1
B_T (T)	1.9	6.0	5.3
I_p (MA)	1.0	6.7	9.0
β_N	3.64	3.7	2.7
f_{BS}	0.51	0.60	0.51
H_{98y2}	1.56	1.6	1.6
H_{EGB}	1.48	1.2	1.0
n_e/n_{GW}	0.46	0.51	0.99
q_{neut} (MW/m ²)	---	2.0	0.55
P_{CD} (MW)	14	71	104
Q_{fus}	---	3.5	3.8

One of the two primary physics objectives of ITER is to achieve $Q_{\text{fus}} = 5$ with ~ 350 MW fusion power under conditions compatible with steady-state operation [14]. While a $Q_{\text{fus}} = 5$ solution at $\beta_N = 3.5$ can be obtained for the hybrid scenario in ITER with a current drive efficiency that is within the capabilities of EC, the density is very high ($n_e/n_{\text{GW}} = 1.5$) and the fusion power of 650 MW exceeds ITER's objective. Therefore, Table 3 gives a more modest steady-state hybrid scenario for ITER with $Q_{\text{fus}} = 3.8$, where the density is fixed to 99% of the Greenwald limit and β_N is lowered to 2.7 to reduce the fusion power to less than 400 MW. The auxiliary heating power for this case, if used to drive current, is sufficient to obtain 100% non-inductive operation.

An important question is whether the stability and confinement assumptions in the zero-dimensional physics model are realistic for the burning plasma regime. A useful stability benchmark for steady-state scenarios is the ideal ballooning beta limit for 99% bootstrap plasmas [15]. Steady-state hybrids on DIII-D stable to the deleterious $m/n=2/1$ mode can reach $\beta_N = 3.64$, which is 75% of the ideal ballooning beta limit for 99% bootstrap plasmas. This is a higher fraction than needed for FNSF, where $\beta_N = 3.7$ is only 67% of the ideal ballooning beta limit for 99% bootstrap plasmas owing to its higher elongation and aspect ratio. Regarding confinement, the issue is whether high H_{98y2} factors can be achieved without the large ExB shear and $T_i > T_e$ typical in present day experiments with strong co-NBI. It turns out that extrapolating from DIII-D to ITER assuming a fixed H_{98y2} factor may actually under predict confinement because the relative gyroradius (ρ^*), collisionality (ν^*) and β scalings of H_{98y2} are too pessimistic. Expressed in dimensionless variables, the H_{98y2} relation scales like $\Omega\tau\alpha(\rho^*)^{-2.7}(\beta)^{-0.9}(\nu^*)^0$ [16]. However, dimensionless parameter scaling experiments in H-mode plasmas find a confinement scaling that can be summarized as $\Omega\tau\alpha(\rho^*)^{-3}(\beta)^0(\nu^*)^{-0.3}$, which we will refer to as electrostatic gyroBohm (EGB) scaling [17]. Since ITER will have smaller ρ^* and ν^* compared to DIII-D, and since steady-state hybrids operate at high β , the projected confinement time on ITER using EGB scaling will be much higher than H_{98y2}

scaling. In fact, using the parameters in Table 3, the projected confinement in ITER assuming EGB scaling (i.e., $H_{\text{EGB}}=1.0$) is equivalent to achieving $H_{98y2}=1.6$, owing to the more pessimistic scaling for the later relation. Further experiments need to measure the ρ^* scaling of confinement in the steady-state hybrid scenario, especially since a Bohm-like scaling was found in joint DIII-D/JET studies in advanced inductive discharges [18].

3. Conclusions

High- β hybrids with realistic current drive efficiencies and competitive fusion energy gain are an alternative to the high- q_{min} AT regime for FNSF and ITER. Experiments in DIII-D have sustained 1.0 MA of plasma current fully non-inductively ($V_{\text{surf}} < 0$ for up to $2 \tau_R$) in the hybrid regime using efficient central current drive from EC and NBI. Although the central current density is calculated to be overdriven, the poloidal magnetic flux pumping in the hybrid scenario maintains q_{min} slightly above 1. The achieved β_N up to 3.64 exceeds the no-wall $n=1$ stability limit and rivals the ideal with-wall $n=1$ limit calculated by DCON. The excellent confinement obtained in these hybrid plasmas, H_{98y2} up to 1.6, may be obtained in ITER even without large ExB shear and $T_i > T_e$ if a viable electrostatic gyroBohm scaling path to the burning plasma regime can be established in the steady-state hybrid scenario. Future experiments will also verify that ELMs can be suppressed in steady-state hybrids around $q_{95}=6$ using $n=3$ resonant magnetic perturbations, as was done previously in inductively-driven hybrids with $q_{95}=3.6$ [19].

Acknowledgements

This material is based upon work supported by the U.S. Department of Energy, Office of Science, Office of Fusion Energy Sciences, using the DIII-D National Fusion Facility, a DOE Office of Science user facility, under Awards DE-FC02-04ER54698, DE-FG02-04ER54761, DE-AC52-07N27344, and DE-FG02-08ER54984. DIII-D data shown in this paper can be obtained in digital format by following the links at https://fusion.gat.com/global/D3D_DMP.

References

- [1] Taylor, T.S. *et al* 1994 *Plasma Phys. Control. Fusion* **36** B229
- [2] Sips, A.C.C. *et al* 2002 *Plasma Phys. Control. Fusion* **44** B69
- [3] Joffrin, E. *et al* 2005 *Nucl. Fusion* **45** 626
- [4] Isayama, A. *et al* 2003 *Nucl. Fusion* **43** 1272
- [5] Luce, T.C. *et al* 2001 *Nucl. Fusion* **41** 1585
- [6] Wade, M.R. *et al* 2005 *Nucl. Fusion* **45** 407
- [7] Petty, C.C. *et al* 2009 *Phys. Rev. Lett.* **102** 045005
- [8] Howl, W. *et al* 1992 *Phys. Fluids B* **4** 1724
- [9] Sabbagh, S.A. *et al* 2004 *Nucl. Fusion* **44** 560
- [10] Heidbrink, W.W. *et al* 2013 *Nucl. Fusion* **53** 093006
- [11] Mikkelsen, D.R. 1989 *Phys. Fluids B* **1** 333
- [12] Glasser, A.H. and Chance M.S. 1997 *Bull. Am. Phys. Soc.* **42** 1848
- [13] Chan, V.S. *et al* 2010 *Fus. Sci. Technol.* **57** 66
- [14] Aymar, R. 2000 *Plasma Physics Control. Fusion* **42** B385
- [15] Lin-Liu, Y.R. and Stambaugh R.D. 2004 *Nucl. Fusion* **44** 548
- [16] ITER Physics Basis Editors *et al* 1999 *Nucl. Fusion* **39** 2137
- [17] Petty, C.C. 2008 *Phys. Plasmas* **15** 080501
- [18] Politzer, P.A. 2010 *Proc. of 23rd IAEA Fusion Energy Conf., Daejeon*, Paper EXC/P2-06
- [19] Petty, C.C. *et al* 2010 *Nucl. Fusion* **50** 022002